

# DNA binding, antioxidant, cytotoxicity (MTT, lactate dehydrogenase, NO), and cellular uptake studies of structurally different nickel(II) thiosemicarbazone complexes: synthesis, spectroscopy, electrochemistry, and X-ray crystallography

R. Prabhakaran · P. Kalaivani · R. Huang ·  
P. Poornima · V. Vijaya Padma · F. Dallemer ·  
K. Natarajan

Received: 2 July 2012 / Accepted: 8 December 2012 / Published online: 29 December 2012  
© SBIC 2012

**Abstract** Three new nickel(II) thiosemicarbazone complexes have been synthesized and characterized by analytical, spectral, and single-crystal X-ray diffraction studies. In complex **1**, the ligand 2-hydroxy-1-naphthaldehydethiosemicarbazone coordinated as a monobasic tridentate donor, whereas in complexes **2** and **3**, the ligands salicylaldehyde-4(*N*)-ethylthiosemicarbazone and 2-hydroxy-1-naphthaldehyde-4(*N*)-ethylthiosemicarbazone coordinated as a dibasic tridentate donor. The DNA binding ability of the complexes in calf thymus DNA was explored by absorption and emission titration experiments. The antioxidant property of the new complexes was evaluated to test their free-radical scavenging ability. In vitro cytotoxicity assays were performed for the new complexes in A549 and HepG2 cell lines. The new compounds overcome cisplatin resistance in the A549 cell line and they were also active in the HepG2 cell line. The cellular uptake study

showed the accumulation of the complexes in tumor cells depended on the nature of the ligand attached to the nickel ion.

**Keywords** Nickel(II) complexes · Thiosemicarbazones · X-ray crystallography · Electrochemistry · DNA binding

## Introduction

Thiosemicarbazones and their metal complexes have become an area of intensive study because of their interesting chemical and structural properties and their wide-ranging biological activities [1–11]. The biological and medicinal properties of thiosemicarbazones depend on the chemical nature of the moiety attached to the C=S carbon atom. The present level of interest in metal complexes of thiosemicarbazones stems from the fact that the biological activities are often attributed to the chelation of thiosemicarbazones to a transition-metal ion [12–19]. In connection with the antitumor activity of thiosemicarbazones, presently there are three main points on which current research is focusing. First, thiosemicarbazones are inhibitors of ribonucleotide reductase activity. Ribonucleotide reductase catalyzes the synthesis of deoxyribonucleotides required for DNA synthesis. Since deoxyribonucleotides are present at extremely low levels in mammalian cells, their synthesis is a crucial and rate-controlling step in the pathway leading to the biosynthesis of DNA. Mammalian ribonucleotide reductase is composed of two dissimilar proteins—R1, which contains polythiols, and R2, which contains non-heme iron and a free tyrosyl radical. Both the R1 subunit and the R2 subunit contribute to the active site of the enzyme [20]. Thiosemicarbazones can destabilize or damage the non-heme-iron-stabilized tyrosyl free radical

R. Prabhakaran (✉) · P. Kalaivani · K. Natarajan (✉)  
Department of Chemistry, Bharathiar University,  
Coimbatore 641046, India  
e-mail: rpnchemist@gmail.com

K. Natarajan  
e-mail: k\_natraj6@yahoo.com

R. Huang  
Department of Chemistry, Michigan State University,  
East Lansing, MI 48824, USA

P. Poornima · V. Vijaya Padma  
Department of Biotechnology, Bharathiar University,  
Coimbatore 641046, India

F. Dallemer  
Laboratoire Chimie Provence-CNRS UMR6264, Université  
of Aix-Marseille I, II and III-CNRS, Campus Scientifique  
de Saint-Jérôme, Avenue Escadrille Normandie-Niemen,  
13397 Marseille Cedex 20, France

and thus inhibit the catalytic function of ribonucleotide reductase. Second, thiosemicarbazones can stabilize cleavable complexes formed by topoisomerase II and DNA, leading to apoptosis [21]. Third, more recently they have been recognized as an inhibitor of ATP-binding cassette transporter proteins, which are responsible for the expulsion from the cell of exogenous molecules that allow cells to develop multidrug resistance. Their action consists in preventing cells from expelling these compounds [22]. The design of compounds able to bind and react with selective nucleotide sequences is of great importance in probing biological processes and in developing therapeutic drugs. Transition-metal compounds that bind to DNA in a covalent or noncovalent fashion or induce DNA strand scission have potential applications as tools for probing biomolecular structure and function and as cytotoxic agents in cancer chemotherapy [23, 24]. Therefore, DNA-targeting drugs remain in the limelight and compounds acting against cancer cells selectively over healthy cells are receiving more attention [25–29]. Despite the therapeutic benefit of platinum-based treatment regimens, the efficacy of platinum drugs is still limited by side effects and intrinsic and acquired resistances [30]. Therefore, the search for new potential platinum drugs is continuing, and some pioneering strategies have emerged. These strategies are represented by the synthesis of nonclassical platinum compounds [31, 32]. With the above-mentioned intention in mind, we synthesized a few platinum-mimic nickel complexes containing biologically active thiosemicarbazones, and this article deals with their synthesis, characterization, and chelating behavior and DNA binding, antioxidant, cytotoxicity, and cellular uptake studies.

## Materials and methods

The ligands 2-hydroxy-1-naphthaldehydethiosemicarbazone ( $H_2L^1$ ), salicylaldehyde-4(*N*)-ethylthiosemicarbazone ( $H_2L^2$ ), and 2-hydroxy-1-naphthaldehyde-4(*N*)-ethylthiosemicarbazone ( $H_2L^3$ )—and the nickel precursor  $[NiCl_2(PPh_3)_2]$  were prepared according to standard literature procedures [33, 34]. All reagents used were Analar grade and were purified and dried according to the standard procedure [35].

### Preparation of $H_2L^1$

Two grams (0.02 mol) of thiosemicarbazide was dissolved in 20 ml hot ethanol and to this was added 3.8 g (0.02 mol) of 2-hydroxy-1-naphthaldehyde in 10 ml ethanol over a period of 10 min with continuous stirring. Further, the mixture was stirred for 5 h at room temperature and a yellow compound began to separate out. The compound

separated was filtered off and washed thoroughly with ethanol and then dried in vacuo. The compound was recrystallized from hot ethanol. The product is soluble in warm acetone, methanol, ethanol, dichloromethane, chloroform, dimethylformamide, and dimethyl sulfoxide (DMSO). Yield: 82 % (4.019 g). Melting point 261 °C. Anal. Calcd for  $C_{12}H_{11}N_3OS$  (%): C, 58.76; H, 4.52; N, 17.13; S, 13.07. Found (%): C, 58.69; H, 4.49; N, 17.05; S, 12.99. IR ( $cm^{-1}$ ) in KBr: 3,446 ( $\nu_{OH}$ ), 1,604 ( $\nu_{C=N}$ ), 1,278 ( $\nu_{C-O}$ ), 815 ( $\nu_{C=S}$ ).  $^1H$  NMR (DMSO- $d_6$ , ppm):  $\delta$  11.5 (s, 1H, OH), 10.7 (s, 1H, NHCS), 8.10 (s, 1H, CH=N), 9.2 (s,  $-NH_2$ ), 7.1–7.8 (m, aromatic protons).

A method similar to that described above was followed to prepare all the other thiosemicarbazone ligands.

### Preparation of $H_2L^2$

This was prepared from ethylthiosemicarbazide (2 g, 0.016 mol) and salicylaldehyde (2.05 g, 0.016 mol). Yield: 80 % (2.856 g). Melting point 160 °C. Anal. Calcd for  $C_{10}H_{13}N_3OS$  (%): C, 53.79; H, 5.87; N, 18.82; S, 14.36. Found (%): C, 53.71; H, 5.83; N, 18.76; S, 14.29. IR ( $cm^{-1}$ ) in KBr: 3,415 ( $\nu_{OH}$ ), 1,621 ( $\nu_{C=N}$ ), 1,276 ( $\nu_{C-O}$ ), 825 ( $\nu_{C=S}$ ).  $^1H$  NMR (DMSO- $d_6$ , ppm):  $\delta$  11.1 (s, 1H, OH), 9.65 (s, 1H, NHCS), 7.87 (s, 1H, CH=N), 8.31 (d, terminal  $-NH$ ), 3.69 (p,  $-CH_2-$ ), 1.25 (t,  $-CH_3$ ), 6.8–7.7 (m, aromatic protons).

### Preparation of $H_2L^3$

This was prepared from ethylthiosemicarbazide (2.98 g, 0.025 mol) and 2-hydroxy-1-naphthaldehyde (4.3 g, 0.025 mol). Yield: 78 % (5.33 g). Melting point 204 °C. Anal. Calcd for  $C_{14}H_{15}N_3OS$  (%): C, 61.51; H, 5.53; N, 15.37; S, 11.73. Found (%): C, 61.48; H, 5.46; N, 15.31; S, 11.66. IR ( $cm^{-1}$ ) in KBr: 3,418 ( $\nu_{OH}$ ), 1,620 ( $\nu_{C=N}$ ), 1,282 ( $\nu_{C-O}$ ), 815 ( $\nu_{C=S}$ ).  $^1H$  NMR (DMSO- $d_6$ , ppm):  $\delta$  11.3 (s, 1H, OH), 10.8 (s, 1H, NHCS), 8.11 (s, 1H, CH=N), 9.18 (d, terminal  $-NH$ ), 3.73 (p,  $-CH_2-$ ), 1.25 (t,  $-CH_3$ ), 7.2–7.8 (m, aromatic protons).

### Preparation of $[Ni(Nap-tsc)(PPh_3)] \cdot Cl \cdot H_2O$ (**1**)

An ethanolic solution (25 ml) of  $[NiCl_2(PPh_3)_2]$  (0.200 g; 0.30 mmol) was slowly added to  $H_2L^1$  (0.075 g; 0.30 mmol) in dichloromethane (25 ml). The mixture was allowed to stand for 4 days at room temperature. The dark-red crystals obtained were filtered off and washed with *n*-hexane. Yield: 86 % (0.159 g). Melting point 284 °C. Anal. Calcd for  $C_{30}H_{26}ClN_3O_2SNiP$  (%): C, 58.33; H, 4.24; N, 6.80; S, 5.19. Found (%): C, 58.28; H, 4.19; N, 6.72; S, 5.12. Fourier transform (FT) IR ( $cm^{-1}$ ) in KBr: 3,160  $cm^{-1}$  ( $\nu_{N(2)H}$ ), 1,600 ( $\nu_{C=N}$ ), 1,351 ( $\nu_{C-O}$ ), 812 ( $\nu_{C=S}$ ),

1,435, 1,094, 697  $\text{cm}^{-1}$  (for  $\text{PPh}_3$ ); UV–vis ( $\text{CH}_2\text{Cl}_2$ ),  $\lambda_{\text{max}}$  (nm): 268 (intraligand transition); 328, 380 (ligand-to-metal charge transfer, LMCT); 417, 686 (forbidden  $d \rightarrow d$  transition).  $^1\text{H}$  NMR (DMSO- $d_6$ , ppm):  $\delta$  8.07 (d, ( $J = 11.2$  Hz) 1H, CH=N), 6.4–7.8 (m, aromatic), 9.4 (s,  $-\text{HN}-\text{C}=\text{S}$ ), 6.48 (br,  $-\text{NH}_2$ ), 6.51 (s,  $-\text{NH}_2$ ).

A similar method was followed to synthesize other complexes.

#### Preparation of $[\text{Ni}(\text{Sal-etsc})(\text{PPh}_3)]$ (2)

This was prepared by the same procedure as described for 1 with  $\text{H}_2\text{L}^2$  (0.068 g; 0.30 mmol). The dark-red crystals obtained were separated and washed with *n*-hexane and dried in a vacuum. It was crystallized using ethanol/chloroform. Yield: 75 % (0.116 g). Melting point 230 °C. Anal. Calcd for  $\text{C}_{28}\text{H}_{26}\text{N}_3\text{OSNiP}$  (%): C, 62.00; H, 4.83; N, 7.75; S, 5.91. Found (%): C, 61.96; H, 4.78; N, 7.72; S, 5.86. FT-IR ( $\text{cm}^{-1}$ ) in KBr: 1,614 ( $\nu_{\text{C}=\text{N}}$ ), 1,348 ( $\nu_{\text{C}-\text{O}}$ ), 753 ( $\nu_{\text{C}-\text{S}}$ ), 1,432, 1,088, 694 (for  $\text{PPh}_3$ ). UV–vis ( $\text{CH}_2\text{Cl}_2$ ),  $\lambda_{\text{max}}$  (nm): 207 (intraligand transition); 303, 382 (LMCT); 420, 440 (forbidden  $d \rightarrow d$  transition).  $^1\text{H}$  NMR (DMSO- $d_6$ , ppm):  $\delta$  9.3 [d, ( $J = 13.2$  Hz) terminal  $-\text{NH}$ ], 8.4 [d, ( $J = 11.0$  Hz)  $-\text{HC}=\text{N}$ ], 6.9–7.8 (m, aromatic protons), 3.32 (q,  $-\text{CH}_2$ ) 1.5 (t, 3H,  $-\text{CH}_3$ ).

#### Preparation of $[\text{Ni}(\text{Nap-etsc})(\text{PPh}_3)]$ (3)

This was prepared by same the procedure as described for 1 with  $\text{H}_2\text{L}^3$  (0.086 g; 0.30 mmol). The dark-red crystals obtained were filtered off and washed with *n*-hexane. Yield: 84 % (0.149 g). Melting point 284 °C. Anal. Calcd for  $\text{C}_{32}\text{H}_{28}\text{N}_3\text{OSNiP}$  (%): C, 64.89; H, 4.76; N, 7.09; S, 5.41. Found (%): C, 64.84; H, 4.70; N, 7.01; S, 5.35. FT-IR ( $\text{cm}^{-1}$ ) in KBr: 1,595 ( $\nu_{\text{C}=\text{N}}$ ), 1,349 ( $\nu_{\text{C}-\text{O}}$ ), 745 ( $\nu_{\text{C}-\text{S}}$ ), 1,437, 1,093, 697 (for  $\text{PPh}_3$ ); UV–vis ( $\text{CH}_2\text{Cl}_2$ ),  $\lambda_{\text{max}}$  (nm): 357, 375, 407 (LMCT); 418 (forbidden  $d \rightarrow d$  transition).  $^1\text{H}$  NMR (DMSO- $d_6$ , ppm):  $\delta$  9.35 [d, ( $J = 11.0$  Hz) terminal  $-\text{NH}$ ], 8.5 [d, ( $J = 8.6$  Hz)  $-\text{HC}=\text{N}$ ], 7.0–8.1 (m, aromatic protons), 3.3 (q,  $-\text{CH}_2$ ), 1.65 (t, 3H,  $-\text{CH}_3$ ).

#### Measurements

IR spectra were measured using KBr pellets with a Nicolet instrument between 400 and 4,000  $\text{cm}^{-1}$ . Elemental analysis of carbon, hydrogen, nitrogen, and sulfur was conducted using a Vario EL III CHNS instrument at the Department of Chemistry, Bharathiar University, Coimbatore, India. The electronic spectra of the complexes were recorded in dichloromethane using a JASCO V-630 spectrophotometer in the 200–800-nm range. Emission spectra were recorded using a JASCO FP-6600 spectrofluorometer.  $^1\text{H}$  NMR spectra were recorded in

DMSO at room temperature with a Bruker 400-MHz instrument, with the chemical shift relative to tetramethylsilane. Melting points were recorded with Lab India apparatus. Single-crystal data collections for the new Ni(II) complexes were performed at 273(2) K with a Bruker SMART 1000 CCD diffractometer using monochromatic Mo  $K\alpha$  ( $\lambda = 0.71073$  Å) radiation. The data were collected and processed using the software program SAINT and the structure was solved and refined by full-matrix least squares on  $F^2$  using SHELXL-97 [36]. Cyclic voltammograms were recorded using a CH Instruments apparatus by using a platinum wire working electrode and a platinum disc counter electrode. All the potentials were referenced to the standard Ag/AgCl electrode and ferrocene was used as an external standard.

#### DNA binding study

Calf thymus DNA (CT-DNA) solutions of various concentrations (0.05–0.5  $\mu\text{M}$ ) dissolved in a phosphate buffer (pH 7) were added to the metal complexes (10  $\mu\text{M}$  dissolved in a DMSO/ $\text{H}_2\text{O}$  mixture). Absorption spectra were recorded after equilibrium had been attained at 20 °C for 10 min. The intrinsic binding constant  $K_b$  was determined using the Stern–Volmer equation [37, 38]:

$$[\text{DNA}]/[\varepsilon_a - \varepsilon_f] = [\text{DNA}]/[\varepsilon_b - \varepsilon_f] + 1/K_b[\varepsilon_b - \varepsilon_f]. \quad (1)$$

where the absorption coefficients  $\varepsilon_a$ ,  $\varepsilon_f$ , and  $\varepsilon_b$  correspond to  $A_{\text{obsd}}/[\text{DNA}]$ , the extinction coefficient for the free complex, and the extinction coefficient for the complex in the fully bound form, respectively. The slope and the intercept of the linear fit of the plot of  $[\text{DNA}]/(\varepsilon_a - \varepsilon_f)$  versus  $[\text{DNA}]$  give  $1/(\varepsilon_b - \varepsilon_f)$  and  $1/K_b(\varepsilon_b - \varepsilon_f)$ , respectively. The intrinsic binding constant  $K_b$  was obtained from the ratio of the slope to the intercept (Table 5) [37]. Emission measurements were conducted using a JASCO FP-6600 spectrofluorometer. Tris(hydroxymethyl)aminomethane buffer was used as a blank to make preliminary adjustments. The excitation wavelength was fixed and the emission range was adjusted before measurements. All measurements were made at 20 °C. For emission spectrum titrations, the concentration of the complex was maintained at 10  $\mu\text{M}$  and the concentration of DNA was varied from 0.05 to 0.5  $\mu\text{M}$ . The emission enhancement factors were measured by comparing the intensities at the emission spectrum maxima under similar conditions. Ethidium bromide (EB)–DNA fluorescence quenching experiments were conducted by adding 0.1  $\mu\text{M}$  solutions of the complexes (10  $\mu\text{l}$  each time) to samples containing 0.5  $\mu\text{M}$  EB, 1.0  $\mu\text{M}$  DNA, and tris(hydroxymethyl)aminomethane buffer (pH 7.2). Before the measurements, the system was shaken and incubated at room temperature for approximately 5 min. The emission was recorded at 530–750 nm.

### Diphenyl-1-picrylhydrazyl radical scavenging assay

The potential antioxidant activity of the new complexes (**1–3**) was evaluated by diphenyl-1-picrylhydrazyl (DPPH) radical scavenging assay according to the procedure described previously with a slight modification [39]. DPPH free radicals are used for rapid analysis of antioxidants. While scavenging the free radicals, the antioxidants donate hydrogen and form a stable DPPH molecule. This reaction involves a color change from purple to yellow that can be measured spectroscopically. Briefly, the complex (25–350  $\mu\text{M}$ ) was added to 2 ml DPPH (0.1 mM in methanol) and was mixed rapidly. The radical scavenging capacity was measured every 10 min using a spectrophotometer by monitoring the decrease in absorbance at 517 nm. The percent DPPH decolorization of the sample was calculated. L-Ascorbic acid was used as a positive control.

### 3-(4,5-Dimethylthiazol-2-yl)-2,5-diphenyltetrazolium bromide assay

The effect of the ligands and the complexes (**1–3**) on the viability of human lung cancer cells (A549) and liver cancer cells (HepG2) was assayed by 3-(4,5-dimethylthiazol-2-yl)-2,5-diphenyltetrazolium bromide (MTT) assay [40]. The cells were seeded at a density of 10,000 cells per well in 200  $\mu\text{l}$  RPMI 1640 medium and were allowed to attach overnight in a  $\text{CO}_2$  incubator, and then the complexes (**1–3**) dissolved in DMSO were added to the cells at a final concentration of 1, 10, 25, and 50  $\mu\text{M}$  in the cell culture medium. After 48 h, the wells were treated with 20  $\mu\text{l}$  MTT (5 mg/ml phosphate-buffered saline, PBS) and incubated at 37  $^\circ\text{C}$  for 4 h. The purple formazan crystals formed were dissolved in 200  $\mu\text{l}$  DMSO and read at 570 nm in a microplate reader.

### Release of lactate dehydrogenase

Lactate dehydrogenase (LDH) activity for the ligands and the complexes was determined by the linear region of a pyruvate standard graph using regression analysis and was expressed as the percentage leakage as described previously [41]. Briefly, to a set of tubes, 1 ml of buffered substrate (lithium lactate) and 0.1 ml of the medium or cell extract were added and the tubes were incubated at 37  $^\circ\text{C}$  for 30 min. After 0.2 ml of NAD solution had been added, the incubation was continued for another 30 min. The reaction was then arrested by adding 0.1 ml 2,4-dinitrophenylhydrazine and the tubes were incubated for a further period of 15 min at 37  $^\circ\text{C}$ . After this, 0.1 ml of medium or cell extract was added to blank tubes after the reaction had been arrested with 2,4-dinitrophenylhydrazine. Then, 3.5 ml

of 0.4 N sodium hydroxide was added to all the tubes. The intensity of the color developed was measured at 420 nm with a Shimadzu UV–vis spectrophotometer. The amount of LDH released was expressed as a percentage.

### Nitric oxide assay

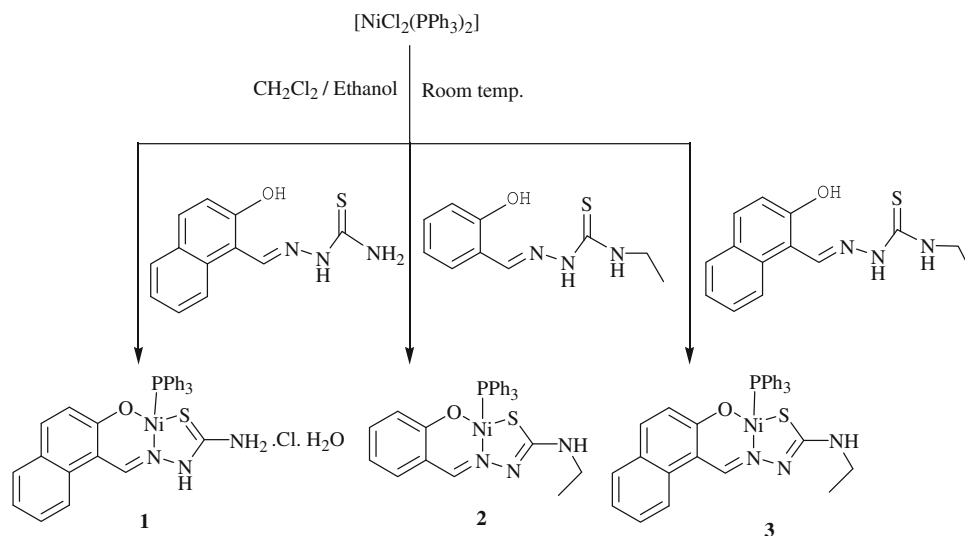
The amount of nitrite was determined by the method of Stueher and Marletta [42]. Nitrite reacts with Griess reagent to give a colored complex which can be measured at 540 nm. To 100  $\mu\text{l}$  of the medium, 50  $\mu\text{l}$  of Griess reagent I was added, mixed, and allowed to react for 10 min. This was followed by addition of 50  $\mu\text{l}$  of Griess reagent II and the reaction mixture was mixed well and incubated for another 10 min at room temperature. The intensity of pink color developed was measured at 540 nm with a MicroQuant plate reader (BioTek Instruments).

### Cellular uptake study

Cellular uptake of the ligands and the complexes (**1–3**) was quantified according to the literature method with a slight modification [43]. Briefly, the lung cancer cells (A549) and liver cancer cells (HepG2) were treated with different concentrations of the ligands and complexes for 4, 12, 24, and 48 h (for A549 cells, 17  $\mu\text{M}$   $\text{H}_2\text{L}^1$ , 20  $\mu\text{M}$   $\text{H}_2\text{L}^2$ , 15  $\mu\text{M}$   $\text{H}_2\text{L}^3$ , 10  $\mu\text{M}$  **1**, 8  $\mu\text{M}$  **2**, 10  $\mu\text{M}$  **3**; for and HepG2 cells, 15  $\mu\text{M}$   $\text{H}_2\text{L}^1$ , 19  $\mu\text{M}$   $\text{H}_2\text{L}^2$ , 14  $\mu\text{M}$   $\text{H}_2\text{L}^3$ , 8  $\mu\text{M}$  **1**, 7  $\mu\text{M}$  **2**, 8  $\mu\text{M}$  **3**). The medium was aspirated and cells were washed three times with ice-cold PBS. Then the cells were lysed with PBS containing 1 % Triton X-100. The concentration of the complexes in the cell lysates was measured with a fluorescence spectrophotometer (JASCO FP-6600) at their maximum excitation/emission wavelengths of 382 nm/482 nm, 340 nm/395 nm, and 432 nm/499 nm, respectively, for complexes **1–3**. To offset the background fluorescence from the cellular components, separate standardization curves were prepared using cellular lysates containing a series of known concentrations of different complexes, and the intracellular concentrations were found using the standard curve.

## Results and discussion

The thiosemicarbazone ligands ( $\text{H}_2\text{L}^1$ – $\text{H}_2\text{L}^3$ ) were reacted with an equimolar amount of  $[\text{NiCl}_2(\text{PPh}_3)_2]$  in 1:1 ethanol/dichloromethane and this resulted in the formation of new complexes (**1–3**) (Scheme 1), where the substituted thiosemicarbazones acted as a dibasic/monobasic tridentate ONS ligand. The analytical data confirmed the stoichiometry of complexes **1–3**. The structures of complexes **1–3** were confirmed by X-ray crystallography. The new

**Scheme 1** Preparation of new nickel(II) complexes

complexes are soluble in common organic solvents such as dichloromethane, chloroform, benzene, acetonitrile, ethanol, methanol, dimethylformamide, and DMSO.

#### IR and electronic absorption spectra

The IR spectra of the thiosemicarbazone ligands ( $H_2L^1$ – $H_2L^3$ ) showed a sharp band at  $1,604$ – $1,621\text{ cm}^{-1}$  corresponding to  $\nu_{C=N}$  of the azomethine group. In the IR spectra of their corresponding complexes (**1**–**3**), this band was shifted to lower frequency ( $1,595$ – $1,614\text{ cm}^{-1}$ ), indicating the coordination of the azomethine nitrogen atom [44, 45]. A broad band corresponding to  $\nu_{O-H}$  appeared in the region from  $3,415$  to  $3,446\text{ cm}^{-1}$  for the ligands, and this disappeared completely after complexation with the nickel(II) ions, showing deprotonation prior to coordination through the oxygen atom in all three complexes. This was further corroborated with the increase in the phenolic C–O stretching frequency ( $1,348$ – $1,351\text{ cm}^{-1}$ ) [46]. The ligand can exist in thione–thiol tautomerization since it contains a thioamide ( $-NH-C=S$ ) functional group. The absence of the  $\nu_{S-H}$  stretching in the region from  $2,500$  to  $2,600\text{ cm}^{-1}$  and presence of  $\nu_{N-H}$  stretching around  $3,140$ – $3,300\text{ cm}^{-1}$  in the IR spectra of the ligands indicate the presence of the thione form in the solid state. This is further inferred from the presence of a strong band in the region from  $815$  to  $825\text{ cm}^{-1}$  due to the  $\nu_{C=S}$  stretching completely disappearing in the spectra of new complexes **2** and **3**, and the appearance of a new band at  $745$ – $753\text{ cm}^{-1}$  due to  $\nu_{C-S}$  indicated the coordination of the  $NH-C=S$  group and subsequent coordination through the sulfur atom [14, 47]. However, in complex **1**, the presence of  $\nu_{N-H}$  stretching at  $3,053\text{ cm}^{-1}$  and the absence of the  $\nu_{S-H}$  stretching frequency evidenced the thione sulfur coordination to the nickel ion [47, 48]. Moreover, the

characteristic absorption bands due to triphenylphosphine were also present in the expected region [49]. The electronic spectra of the new nickel(II) complexes displayed four to five bands in the region around  $207$ – $686\text{ nm}$ . The band at  $207$ – $268\text{ nm}$  has been assigned to an intraligand transition, the band at  $303$ – $407\text{ nm}$  has been assigned to an LMCT ( $s \rightarrow d$ ), and the shoulder at  $417$ – $686\text{ nm}$  has been assigned to a forbidden  $d \rightarrow d$  transition [50, 51].

#### $^1H$ NMR spectra

The  $^1H$  NMR spectra of the ligands ( $H_2L^1$ – $H_2L^3$ ) and the corresponding complexes (**1**–**3**) recorded in DMSO showed all the expected signals. The sharp singlet observed at  $\delta$   $11.1$ – $11.5$  ppm in the spectra of the free ligands due to the phenolic–OH proton completely disappeared in the spectra of all three complexes, confirming the involvement of phenolic oxygen in coordination. The spectra of  $H_2L^2$  and  $H_2L^3$  showed a singlet at  $\delta$   $9.65$ – $10.8$  ppm corresponding to the  $N(2)H-C=S$  proton [52], but in complexes **2** and **3** there was no resonance attributable to  $N(2)H$ , indicating coordination of the ligand in the anionic form after deprotonation at  $N(2)$ . The spectrum of  $H_2L^1$  showed a sharp singlet at  $\delta$   $10.7$  ppm corresponding to the  $N(2)H-C=S$  group, but this disappeared and a new singlet appeared at  $\delta$   $9.4$  ppm in complex **1**, indicating the coordination of the thionic form of the ligand to the nickel ion [53]. In complexes **2** and **3**, two doublets observed at  $\delta$   $8.4$ – $8.5$  ppm and  $\delta$   $9.3$ – $9.35$  ppm were assigned to azomethine and terminal  $-NH$  group protons [51, 54]. In complex **1**, a doublet corresponding to an azomethine proton was observed at  $\delta$   $8.07$  ppm and two broad singlets appeared at  $\delta$   $6.48$  ppm and  $\delta$   $6.51$  ppm, which were assigned to  $NH_2$  group protons. The doublets observed for azomethine and terminal  $-NH$  group protons may be due to the coupling

with a phosphorus atom of the triphenylphosphine and the restricted rotation of the C–N bond of the ligand, respectively [18, 54]. Further, the spectra of all three complexes showed a series of overlapping multiplets for aromatic protons at  $\delta$  6.4–8.1 ppm [55]. In addition, a quartet was observed around  $\delta$  3.30–3.32 ppm corresponding to  $-\text{CH}_2-$  group protons and a triplet was observed at  $\delta$  1.5–1.65 ppm due to  $\text{CH}_3$  group protons of the ligands in complexes 2 and 3 [56].

#### Description of the crystal structures

The crystal structures of complexes 1–3 along with their numbering schemes and their hydrogen-bonding diagrams are given in Figs. 1, 2, and 3. Crystallographic data and bond parameters are given in Tables 1 and 2. Complexes 1 and 3 crystallized in monoclinic space group  $P2_1/c$  and complex 2 crystallized in orthorhombic space group  $P2_12_12_1$ .

In complex 1, the ligand ( $\text{H}_2\text{L}^1$ ) is coordinated to nickel by using its phenolic oxygen, N1 nitrogen, and thione sulfur atoms and behaved as a monobasic tridentate donor by forming a six-membered ring and a five-membered ring with a bite angle of  $88.16(5)^\circ$  (S–Ni–N). The presence of a chloride ion outside the coordination sphere compensated for the charge of nickel as  $\text{Ni}^{2+}$ , resulting in the formation of ionic compound 1. From the  $^1\text{H}$  NMR spectral studies, there was a detectable proton signal at  $\delta$  9.4 ppm corresponding to the  $\text{N}(2)\text{H}-\text{C}=\text{S}$  group. However, the position of this proton (hydrogen) could not be located in the X-ray crystallographic analysis. While dealing the hydrogen-bonding interaction, we found the donor–acceptor distance

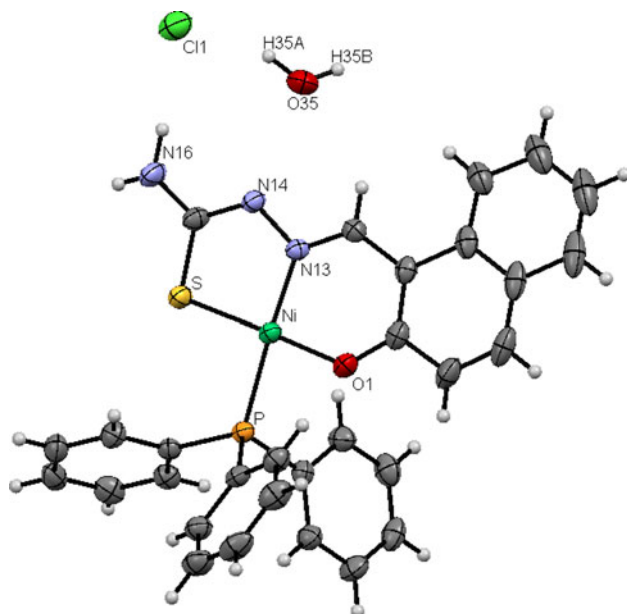


**Fig. 1** ORTEP diagram of  $[\text{Ni}(\text{H-Nap-tsc})(\text{PPh}_3)]\cdot\text{Cl}\cdot\text{H}_2\text{O}$  (1)

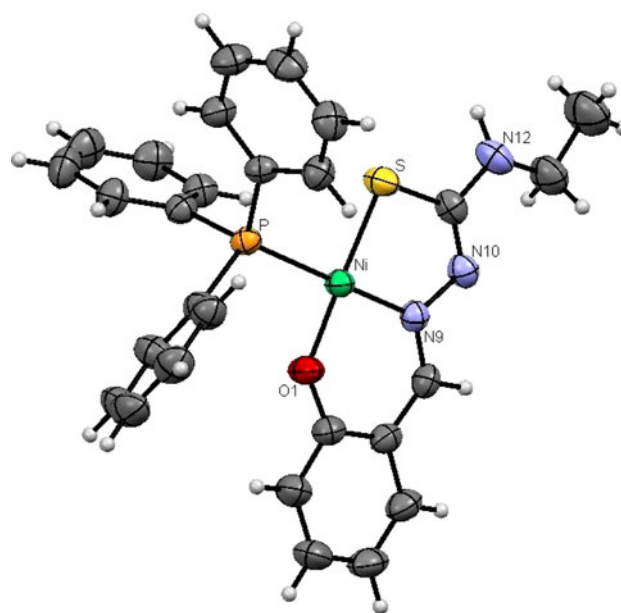


**Fig. 2** ORTEP diagram of  $[\text{Ni}(\text{Sal-etsc})(\text{PPh}_3)]$  (2)

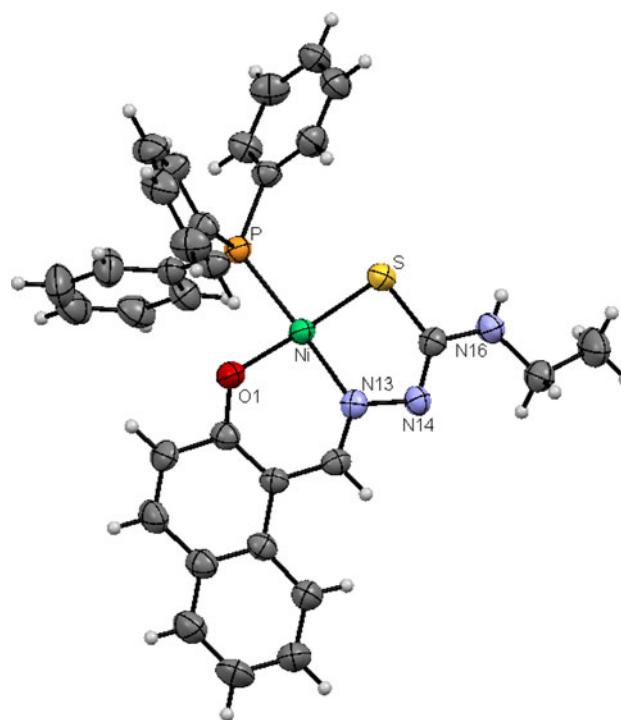


**Fig. 3** ORTEP diagram of  $[\text{Ni}(\text{Nap-etsc})(\text{PPh}_3)]$  (3)

( $2.763 \text{ \AA}$ ) corresponding to the  $\text{N}(14)\cdots\text{O}(35)$  bond between the imine nitrogen and the oxygen atom of the water which came through the solvent of crystallization. The water molecule may be from the ethanol which was used for the preparation of the complex. The presence of four hydrogen bonds creates a 2D network in the complex: the first one between one of the hydrogen atoms of the

**Table 1** Crystal data of the new nickel(II) thiosemicarbazone complexes

	[Ni(H-Nap-tsc)(PPh <sub>3</sub> )]·Cl·H <sub>2</sub> O (1)	[Ni(Sal-etsc)(PPh <sub>3</sub> )] (2)	[Ni(Nap-etsc)(PPh <sub>3</sub> )] (3)
Empirical formula	C <sub>30</sub> H <sub>26</sub> ClN <sub>3</sub> NiO <sub>2</sub> PS	C <sub>28</sub> H <sub>26</sub> N <sub>3</sub> NiOPS	C <sub>32</sub> H <sub>28</sub> N <sub>3</sub> NiOPS
Formula weight	617.73	542.26	592.31
Temperature	173(2) K	173(2) K	173(2) K
Wavelength	0.71073 Å	0.71073 Å	0.71073 Å
Crystal system	Monoclinic	Orthorhombic	Monoclinic
Space group	<i>P2<sub>1</sub>/c</i>	<i>P2<sub>1</sub>2<sub>1</sub>2<sub>1</sub></i>	<i>P2<sub>1</sub>/c</i>
Unit cell dimensions			
<i>a</i>	12.755(3) Å	10.565(2) Å	13.292(3) Å
<i>b</i>	22.037(4) Å	13.185(3) Å	11.542(2) Å
<i>c</i>	10.309(2) Å	18.174(4) Å	19.039(4) Å
$\alpha$	90°	90°	90°
$\beta$	97.19(3)°	90°	108.05(3)°
$\gamma$	90°	90°	90°
Volume	2,874.8(10) Å <sup>3</sup>	2,531.6(9) Å <sup>3</sup>	2,777.2(10) Å <sup>3</sup>
<i>Z</i>	4	4	4
Density (calculated)	1.427 Mg m <sup>-3</sup>	1.423 Mg m <sup>-3</sup>	1.417 Mg m <sup>-3</sup>
Absorption coefficient	0.929 mm <sup>-1</sup>	0.939 mm <sup>-1</sup>	0.863 mm <sup>-1</sup>
<i>F</i> (000)	1,276	1,128	1,232
$\theta$ range for data collection	1.61–28.23°	1.91–28.19°	1.61–28.25°
Index ranges	−16 ≤ <i>h</i> ≤ 16, −29 ≤ <i>k</i> ≤ 29, −13 ≤ <i>l</i> ≤ 13	−13 ≤ <i>h</i> ≤ 13, −16 ≤ <i>k</i> ≤ 16, −22 ≤ <i>l</i> ≤ 23	−17 ≤ <i>h</i> ≤ 17, −15 ≤ <i>k</i> ≤ 15, −25 ≤ <i>l</i> ≤ 25
Collected/unique reflections	33,759/6,922 ( <i>R</i> <sub>int</sub> = 0.0265)	27,751/5,831 ( <i>R</i> <sub>int</sub> = 0.0262)	28,619/6,667 ( <i>R</i> <sub>int</sub> = 0.0250)
Completeness to $\theta$	28.23, 97.6 %	28.19, 96.3 %	28.25, 96.9 %
Refinement method	Full-matrix least squares on <i>F</i> <sup>2</sup>	Full-matrix least squares on <i>F</i> <sup>2</sup>	Full-matrix least squares on <i>F</i> <sup>2</sup>
Data/restraints/parameters	6,922/0/359	5,831/0/324	6,667/0/356
Goodness of fit on <i>F</i> <sup>2</sup>	0.828	0.567	1.356
Final <i>R</i> indices [ <i>I</i> > 2 $\sigma$ ( <i>I</i> )]	<i>R</i> <sub>1</sub> = 0.0404, <i>wR</i> <sub>2</sub> = 0.0962	<i>R</i> <sub>1</sub> = 0.0285, <i>wR</i> <sub>2</sub> = 0.0670	<i>R</i> <sub>1</sub> = 0.0469, <i>wR</i> <sub>2</sub> = 0.1616
<i>R</i> indices (all data)	<i>R</i> <sub>1</sub> = 0.0289, <i>wR</i> <sub>2</sub> = 0.1061	<i>R</i> <sub>1</sub> = 0.0229, <i>wR</i> <sub>2</sub> = 0.0714	<i>R</i> <sub>1</sub> = 0.0408, <i>wR</i> <sub>2</sub> = 0.1646
Largest diffraction peak and hole	0.357 and −0.270 e <sup>-</sup> Å <sup>-3</sup>	0.228 and −0.149 e <sup>-</sup> Å <sup>-3</sup>	0.848 and −0.516 e <sup>-</sup> Å <sup>-3</sup>

**Table 2** Selected bond lengths (Å) and angles (°) of the new nickel (II) thiosemicarbazone complexes

	1	2	3
Bond lengths			
Ni–O	1.8471(13)	1.8347(14)	1.8445(19)
Ni–N	1.8734(14)	1.8848(15)	1.8848(15)
Ni–S	2.1528(6)	2.1426(6)	2.1426(6)
Ni–P	2.2114(6)	2.2103(6)	2.2000(7)
Bond angles			
O–Ni–N	93.26(6)	94.98(6)	95.20(8)
S–Ni–P	94.20(3)	91.59(2)	92.95(3)
N–Ni–S	88.16(5)	87.09(5)	87.80(7)
O–Ni–P	84.49(5)	87.00(5)	84.13(6)
N–Ni–P	176.32(4)	172.84(5)	174.68(6)
O–Ni–S	177.47(4)	174.30(6)	176.91(6)

amine nitrogen and the chloride ion, the second one between the chloride ion and one of the hydrogen atoms (H35A) of the water molecule, the third one between the oxygen atom of the water molecule and the imine nitrogen, and the fourth one between H35(B) of the water molecule and the second chloride ion (Table 3). The S(1)–Ni–O(1) [177.46(4)°] and P(1)–Ni–N(13) [176.32(4)°] bond angles deviate significantly from the ideal angle of 180°, causing significant distortion in the square plane.

The ligand H<sub>2</sub>L<sup>2</sup> coordinated to the metal by losing two protons from its tautomeric thiol form and phenolic –OH in complex **2** and acts as a dibasic tridentate ligand via the thiolate sulfur, phenolic oxygen, and hydrazinic nitrogen atoms by forming a six-membered ring and a five-membered ring with bite angle of 87.08(5)° (S–Ni–N). In this complex, the S(1)–Ni–O(1) [174.30(5)°] and P(1)–Ni–N(1)

**Table 3** Hydrogen bonds for complex **1**

D–H...A	<i>d</i> (D–H) (Å)	<i>d</i> (H...A) (Å)	<i>d</i> (D...A) (Å)	∠(D–H...A) (°)
N16(A)–H16(B)···Cl1(A)	0.985	2.245	3.227	174.78
O35(A)–H35(B)···Cl1(B)	0.860	2.359	3.216	175.22
O35(A)–H35(A)···Cl1(A)	0.936	2.219	3.113	159.41
N14(A)···O(35)	–	–	2.763	–

Symmetry operation: (*x*, *y*, *z*); (–*x*, +1/2 + *y*, 1/2 – *z*); (–*x*, –*y*, –*z*); (*x*, 1/2 – *y*, 1/2 + *z*)

A acceptor, D donor

[172.84(5)°] bond angles deviate considerably from the ideal angle of 180°. The variation in the bonding parameters indicates that there is considerable distortion in the NiSNOP core around nickel. The C–S bond distance of 1.753(2) Å indicates that the ligand is bound to nickel in the thiolate form [57]. In complex **3**, the ligand (H<sub>2</sub>L<sup>3</sup>) coordinated to the metal in an ONS fashion and acted as a dibasic tridentate ligand coordinating through thiolate sulfur, phenolic oxygen, and hydrazinic nitrogen atom, by forming a six-membered ring and a five-membered ring with a bite angle of 87.80(7)° (S–Ni–N). The S(1)–Ni–O(1) (176.9°) and P(1)–Ni–N(1) (174.68°) bond angles showed significant distortion around the nickel atom. The C–S bond distance of 1.7490 Å found for the complex indicates that the ligand bound to nickel in the thiolate form. In all three complexes, the observed Ni–N bond distance of 1.8734(14)–1.885(2) Å is a bit shorter compared with the bond distances in already reported nickel(II) complexes, which may be due to the strong  $\pi$  interaction between the imine nitrogen and nickel. All other observed bond lengths are within the range of those of already reported complexes [58–61]. The variation in the bonding parameters indicates that there is considerable distortion from a square planar geometry in the NiSNOP core around nickel.

### Electrochemistry

Electron transfer properties of the new Ni(II) complexes were studied by cyclic voltammetry using dichloromethane as a solvent, platinum wire as the working electrode, and a platinum disc as the counter electrode and 0.1 M tetrabutylammonium perchlorate as the supporting electrolyte at a scan rate of 100 mV s<sup>–1</sup>. All potentials were referenced to the Ag/AgCl electrode. Ferrocene was used as an external standard. These complexes were electroactive in the  $\pm 2.0$  V sweep range. Complex **1** showed a quasi-reversible oxidation at 0.503 V with peak-to-peak separation of 602 mV and reversible ligand reduction at –1.6575 V with peak-to-peak separation of 75 mV. It also exhibited irreversible ligand oxidation at 0.920 V (Table 4). Complex **2** showed reversible oxidation and quasi-reversible reduction on both sides with peak-to-peak separations of 59 and

125 mV, respectively. Generally, the redox processes are defined by the coordination number, stereochemistry, and hard/soft donor character of the ligands. However, owing to inherent difficulties in relating the coordination number and stereochemistry of the species present in solution, the redox process is generally described in terms of the nature of the ligands present [62]. Patterson and Holm [63] have shown that soft donor ligands tend to show more positive  $E_{1/2}$  values and hard donor ligands tend to show more negative  $E_{1/2}$  values. For this complex, the  $E_{1/2}$  values observed at 0.7734 and –0.3422 V for the oxidation and reduction processes, respectively, are similar to the values observed for other nickel(II) complexes [64]. In addition, it showed a quasi-reversible ligand reduction at –1.3482 V with a peak-to-peak separation of 545 mV. The cyclic voltammogram of **3** showed a one-electron reversible reduction at  $E_{1/2}$  of –0.2122 V [65]. The quasi-reversible ligand reduction was observed at  $E_{1/2}$  of –1.0424 V with a peak-to-peak separation of 453 mV (Fig. 4) [66]. In addition, the complex exhibited an irreversible oxidation at  $E_{1/2}$  of 0.774 V.

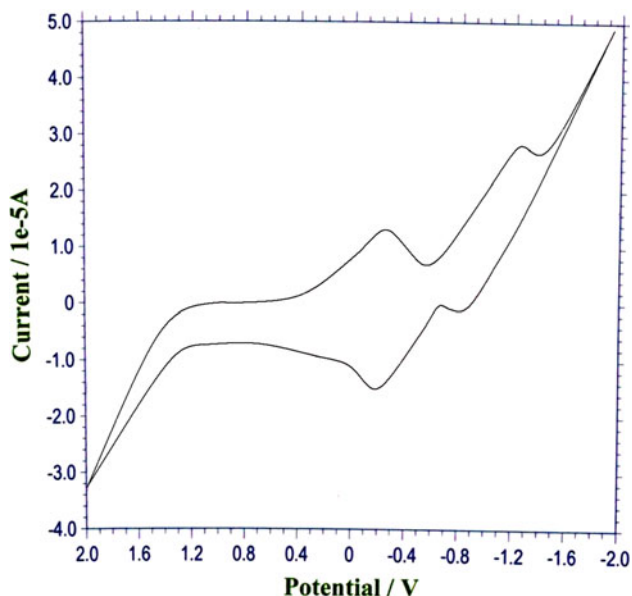
### DNA binding studies

Absorption titration experiments were performed to study the DNA binding property of the new nickel(II) complexes (**1–3**). The absorption spectra of the complexes at constant concentration (10  $\mu$ M) in the presence of different concentrations of CT-DNA (0.05–0.50  $\mu$ M) are given in Fig. 5. The absorption spectra of complex **1** consist of two resolved bands centered at 271 nm (intraligand transition) and 325 nm (LMCT). As the DNA concentration is increased, hyperchromism ( $A = 0.2223$ – $1.4465$ ) with a blueshift of 10 nm (up to 261 nm) was observed in the intraligand band. The LMCT band at 325 nm showed modest hypochromism ( $A = 0.1858$ – $0.1431$ ) with negligible shifts in the wavelength. The binding behavior of complexes **2** and **3** is also quite similar. Complex **2** exhibited hyperchromism in the intraligand band at 269 nm ( $A = 0.1945$ – $1.5374$ ) with 8-nm blueshift and hypochromism at 325 nm (LMCT) ( $A = 0.1840$ – $0.1100$ ). The spectra of complex **3** consist of two resolved bands centered at 273 nm (intraligand transition) and 379 nm (LMCT). As the DNA concentration is increased, hyperchromism ( $A = 0.2835$ – $2.2745$ ) with a blueshift of 13 nm was observed in the intraligand band. The LMCT band at 379 nm ( $A = 0.1421$ – $0.1171$ ) showed hypochromism with negligible shifts in the wavelength. The observed hyperchromic effect with a blueshift suggested that the new complexes bind to CT-DNA by external contact, possibly due to electrostatic binding [67, 68].

The intrinsic binding constant  $K_b$  is a useful tool to monitor the magnitude of the strength with which

**Table 4** Electrochemical data of the new nickel(II) complexes

Complex	Ni <sup>II</sup> –Ni <sup>III</sup> oxidation				Ni <sup>II</sup> –Ni <sup>I</sup> reduction				Ligand reduction				Ligand oxidation			
	<i>E</i> <sub>pa</sub> (V)	<i>E</i> <sub>pc</sub> (V)	<i>E</i> <sub>1/2</sub> (V)	Δ <i>E</i> <sub>p</sub> (mV)	<i>E</i> <sub>pa</sub> (V)	<i>E</i> <sub>pc</sub> (V)	<i>E</i> <sub>1/2</sub> (V)	Δ <i>E</i> <sub>p</sub> (mV)	<i>E</i> <sub>pa</sub> (V)	<i>E</i> <sub>pc</sub> (V)	<i>E</i> <sub>1/2</sub> (V)	Δ <i>E</i> <sub>p</sub> (mV)	<i>E</i> <sub>pa</sub> (V)	<i>E</i> <sub>pc</sub> (V)	<i>E</i> <sub>1/2</sub> (V)	Δ <i>E</i> <sub>p</sub> (mV)
<b>1</b>	0.202	0.804	0.503	602	–	–	–	–	–1.695	–1.620	–0.6575	75	0.920	–	–	–
<b>2</b>	0.744	0.803	0.774	59	–0.405	–0.280	–0.342	125	–1.621	–1.076	–1.348	545	–	–	–	–
<b>3</b>	–	–	–	–	–0.262	–0.162	–0.212	100	–1.269	–0.816	–1.042	453	–	–	–	–

**Fig. 4** Cyclic voltammogram of complex **3**

compounds bind with CT-DNA (Table 5). It can be determined by monitoring the changes in the absorbance in the intraligand band at the corresponding  $\lambda_{\max}$  with increasing concentration of DNA and is given by the ratio of slope to the *y* intercept in plots of  $[\text{DNA}]/(\epsilon_a - \epsilon_f)$  versus  $[\text{DNA}]$  (insets in Fig. 5).

In the emission spectra, complex **1** exhibited fluorescence at 299 nm (Fig. 6). On addition of CT-DNA to this complex, the fluorescence intensity decreased ( $I = 177.71\text{--}83.84$ ) without any shift in wavelength. Similarly, complexes **2** and **3** showed hypochromism at 430 nm ( $I = 113.66\text{--}82.11$ ) with a 9-nm blueshift and at 442 nm ( $I = 377.70\text{--}184.61$ ) with a 4 nm redshift, respectively. The marked decreases in the fluorescence intensity of the new complexes indicate the intercalative binding mode of DNA.

To further confirm the interaction between complexes **1–3** and CT-DNA, competitive binding studies using EB (a planar intercalating nonemissive molecule which fluoresces intensely when bound to DNA) were conducted. The emission intensity of EB is used as a structural probe as EB shows reduced emission intensity in buffer solution because of solvent quenching or because of a photoelectron transfer mechanism [69] and enhancement of emission

intensity when bound intercalatively to DNA. When complexes **1–3** were added to DNA pretreated with EB, the DNA-induced emission intensity at 604 nm was decreased (Fig. 7). This indicated that the complexes could replace EB from the EB–DNA system. Such a characteristic change is often observed in intercalative DNA interactions. The Stern–Volmer quenching constant,  $K_{SV}$ , obtained as the slope of  $I_0/I$  versus the concentration of the quencher was evaluated for complexes **1–3** and was found to be  $9.52 \times 10^3$ ,  $3.35 \times 10^3$ , and  $8.27 \times 10^3$ , respectively. A large decrease in emission intensity suggests stronger binding to CT-DNA [70].

#### DPPH radical scavenging assay

The free-radical scavenging activity of new nickel(II) complexes **1–3** was tested by the ability to bleach the stable radical DPPH. This assay provided information on the reactivity of the compounds with a stable free radical. Because of the odd electron, DPPH shows a strong absorption band at 517 nm [14]. As this electron becomes paired off in the presence of a free-radical scavenger, the absorption vanishes, and the resulting decolorization is stoichiometric with respect to the number of electrons taken up. The new complexes exhibited a significant DPPH radical scavenging effect greater than that of well-established vitamin C, a reference drug established elsewhere [71, 72]. The free-radical scavenging activity of the complexes increased with increase in the concentration of the complexes, and 59, 73, and 53.3 % activity was shown at 250  $\mu\text{g/ml}$  concentration of complexes **1**, **2**, and **3**, respectively (Fig. 8). The observed antioxidant activity of the nickel complex may be due to the neutralization of the free-radical character of DPPH by transfer of either an electron or a hydrogen atom [73]. It could also be due to the inhibition of lipid peroxidation as indicated earlier [74]. Among the three complexes, complex **2** showed the best activity.

#### MTT assay

The ligands, complexes **1–3**, and the standard cisplatin were evaluated for their cytotoxicity in two different human tumor cell lines (A549 and HepG2) by means of a

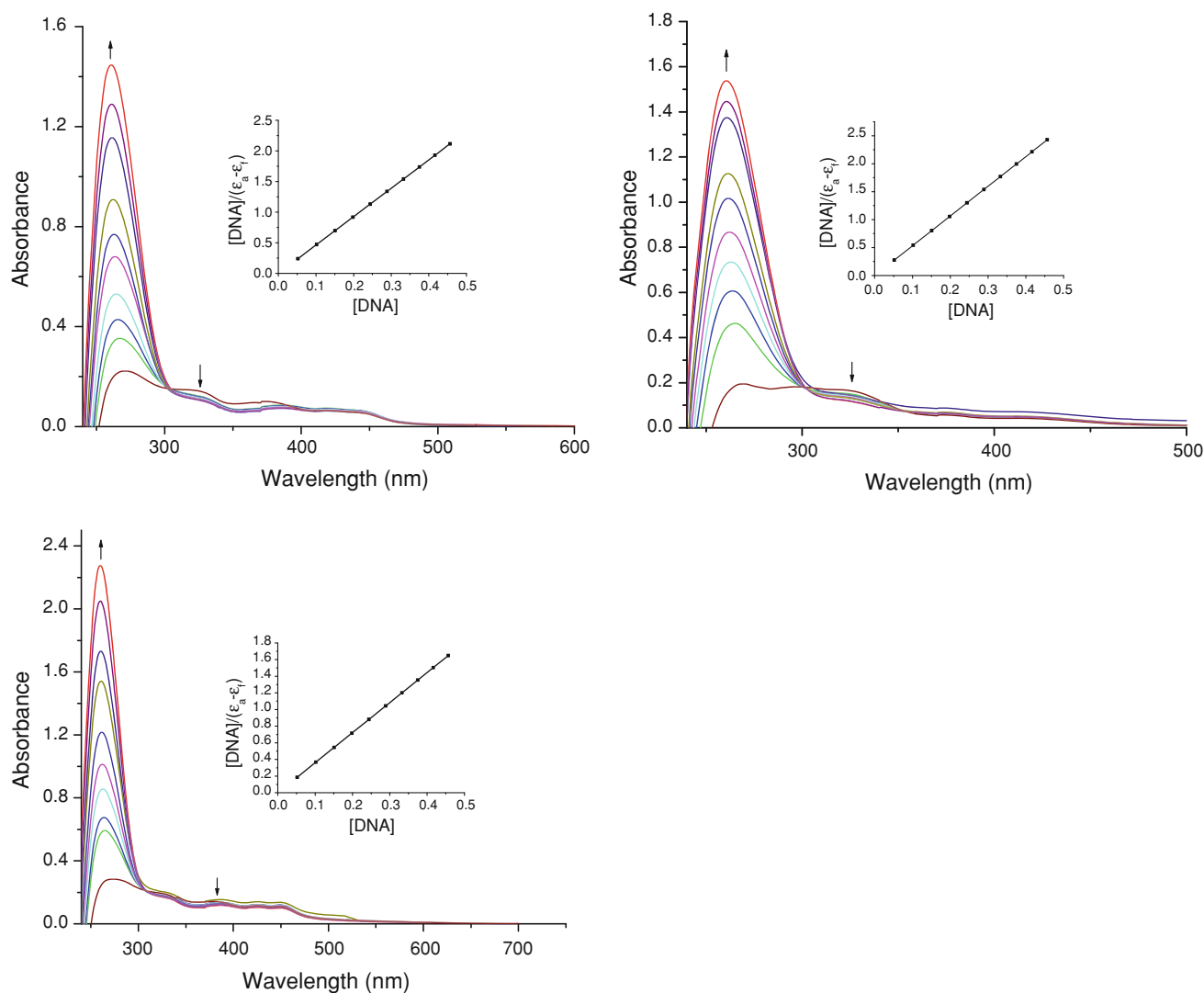


**Fig. 5** Absorption titration spectra of complexes **1–3** with increasing concentrations (0.05–0.5  $\mu\text{M}$ ) of calf thymus DNA (CT-DNA; phosphate buffer, pH 7). The *insets* show binding isotherms with CT-DNA

**Table 5** Binding constant for interaction of nickel(II) complexes with calf thymus DNA (CT-DNA)

System	$K_b$ ( $\times 10^5 \text{ M}^{-1}$ )
CT-DNA + <b>1</b>	2.22343
CT-DNA + <b>2</b>	8.79644
CT-DNA + <b>3</b>	1.12006

colorimetric assay (MTT assay) which measures mitochondrial dehydrogenase activity as an indication of cell viability, and the cells were evaluated after 48 h. All the ligands and complexes showed activity and their corresponding  $\text{IC}_{50}$  values, corresponding to inhibition of cancer cell growth at the 50 % level, are shown in Fig. 9. All the complexes have cytotoxic potencies, with  $\text{IC}_{50}$  values generally in the low micromolar range. As a general observation, complex **2** is more active than the other

complexes in the cell lines tested, and it exhibited much better activity than cisplatin in the A549 cell line. Between cell lines, there is a weakly discernible trend in the activities the complexes showed against the liver cancer cell line (HepG2). By comparing the cytotoxicity with that of the conventional standard cisplatin, we found that the complexes exhibited excellent activity in the lung cancer cell line (A549). In the liver cancer cell line the complexes exhibited higher activity than cisplatin but not the maximum observed as in the lung cancer cell line. In addition, the activities of the complexes were much higher than those of their parent ligands.

#### LDH release

LDH is a membrane-bound enzyme and its presence is a measure of cell membrane integrity. Leakage of LDH into

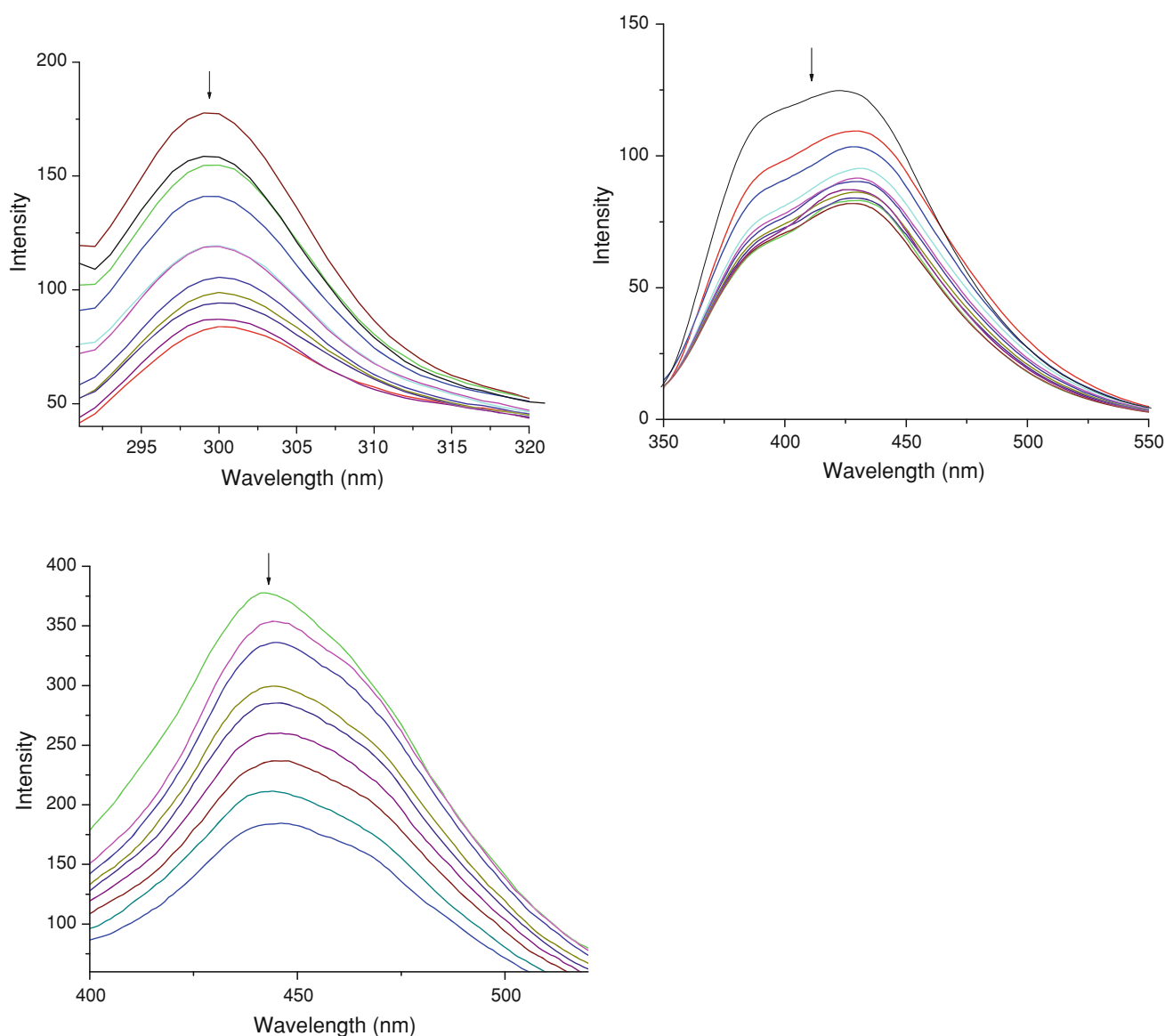


**Fig. 6** Changes in the emission spectra of complexes **1–3** with increasing concentrations (0.05–0.5  $\mu\text{M}$ ) of CT-DNA (phosphate buffer, pH 7)

the culture medium is often associated with membrane damage and therefore serves as a means to detect apoptosis. In this study, significant levels of LDH leakage were observed in the cell culture medium of A549 and HepG2 cell lines when they are treated with the respective  $\text{IC}_{50}$  concentrations (for A549, 17  $\mu\text{M}$   $\text{H}_2\text{L}^1$ , 20  $\mu\text{M}$   $\text{H}_2\text{L}^2$ , 15  $\mu\text{M}$   $\text{H}_2\text{L}^3$ , 10  $\mu\text{M}$  **1**, 8  $\mu\text{M}$  **2**, 10  $\mu\text{M}$  **3**; for HepG2, 15  $\mu\text{M}$   $\text{H}_2\text{L}^1$ , 19  $\mu\text{M}$   $\text{H}_2\text{L}^2$ , 14  $\mu\text{M}$   $\text{H}_2\text{L}^3$ , 8  $\mu\text{M}$  **1**, 7  $\mu\text{M}$  **2**, 8  $\mu\text{M}$  **3**) for 48 h (Fig. 10). There was a significant variation in the LDH release caused by the ligands and the complexes when comparing among them and with the control. However, there was no appreciable difference among the complexes on rupturing the cell membrane. The LDH release further confirmed the higher impact of the

complexes on lung and liver cancer cell lines by comparing them with the ligands and the control.

#### Nitric oxide assay

Nitric oxide has been shown to directly inhibit methionine adenosyl transferase, leading to glutathione depletion, and its reaction with superoxide generates the strong oxidant peroxynitrite, which can initiate lipid peroxidation or cause direct inhibition of the mitochondrial respiratory chain [75]. Hence the presence of nitric oxide is also an important measure of cytotoxicity. In this study it is obvious that the treatment with the ligands and their complexes significantly increased nitric oxide levels in the human lung and liver

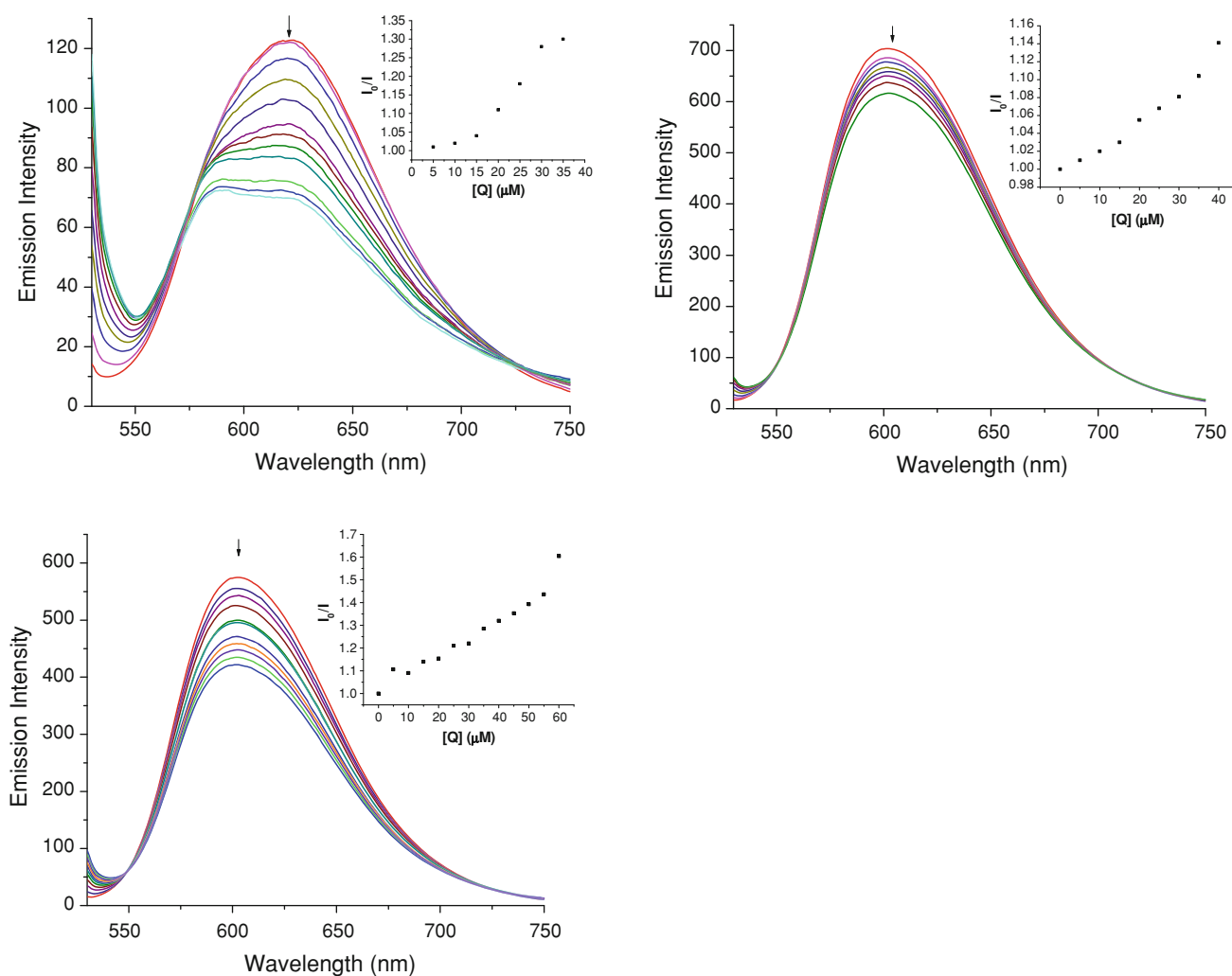


**Fig. 7** Emission spectra of ethidium bromide bound to DNA in the presence of complexes **1–3** in tris(hydroxymethyl)aminomethane–HCl buffer (pH 7.2). Arrows indicate the intensity changes upon

increasing the concentration of the complexes. *Inset* fluorescence quenching curve of DNA-bound ethidium bromide with the complexes

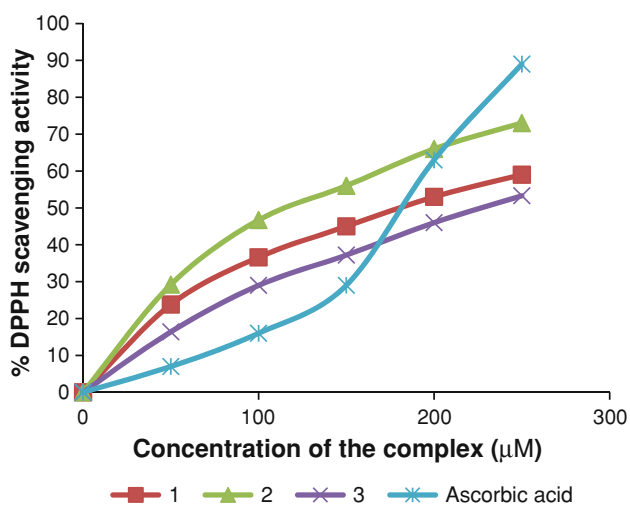


**Fig. 8** Diphenyl-1-picrylhydrazyl (DPPH) scavenging activity of new Ni(II) complexes **1–3**

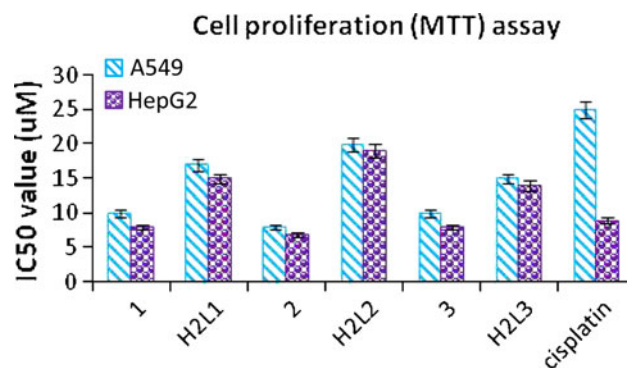


**Fig. 9** The  $IC_{50}$  values (50 % inhibition of cell growth for 48 h) for the ligands, complexes **1–3**, and cisplatin. *MTT* 3-(4,5-dimethylthiazol-2-yl)-2,5-diphenyltetrazoliumbromide

cancer cell lines tested (A549 and HepG2) when compared with the control group (Fig. 11). The results indicate the very poor radical scavenging activity of the ligands.

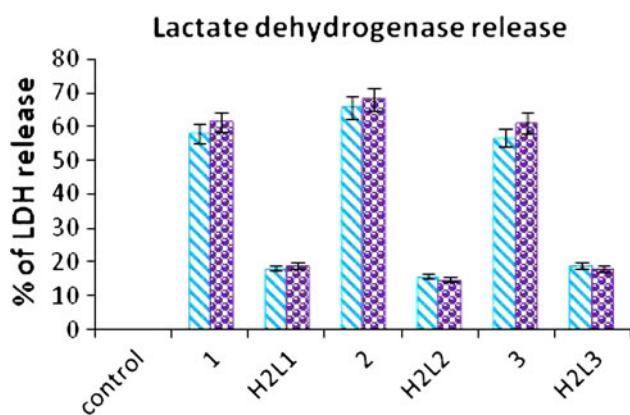


**Fig. 10** Percentage of lactate dehydrogenase (*LDH*) released by the human cancer cell lines A549 and HepG2 after an incubation period of 48 h with the ligands (for A549, 17  $\mu\text{M}$   $\text{H}_2\text{L}^1$ , 20  $\mu\text{M}$   $\text{H}_2\text{L}^2$ , 15  $\mu\text{M}$   $\text{H}_2\text{L}^3$ ; for HepG2, 15  $\mu\text{M}$   $\text{H}_2\text{L}^1$ , 19  $\mu\text{M}$   $\text{H}_2\text{L}^2$ , 14  $\mu\text{M}$   $\text{H}_2\text{L}^3$ ) and complexes 1–3 (IC<sub>50</sub> for A549, 10  $\mu\text{M}$  1, 8  $\mu\text{M}$  2, 10  $\mu\text{M}$  3; IC<sub>50</sub> for HepG2, 8  $\mu\text{M}$  1, 7  $\mu\text{M}$  2, 8  $\mu\text{M}$  3). Error bars represent the standard error of the mean ( $n = 6$ )

### Cellular uptake study

To explain the significant difference in the cytotoxicities, uptake studies were performed in A549 and HepG2 cell lines. The amount of compounds which were taken up by both liver and lung carcinoma cells in the different incubation periods (4, 12, 24, and 48 h) was investigated in triplicate as shown in Figs. 12 and 13. The intracellular concentration of the test compounds was found using the method described in “Materials and methods.” The intracellular concentration of a specific drug is vital in the design of a therapeutic drug. The percentage of cellular uptake was higher in complex 3, followed by complexes 1 and 2 and then the ligands. The lower percentage of cellular uptake of the ligands reflects the meager uptake of the compounds into the cells. Moreover, the intracellular uptake of the complexes was investigated in the presence of glutathione as an antioxidant, and significant reduction in the cellular uptake was observed. This may be due to the displacement of the complexes by glutathione in the cells [76]. The greater electron-withdrawing effect of the chelating ligand in 3 increases the cellular uptake level by increasing the lipophilic character of the central metal atom, which subsequently favors permeation through the lipid layer of the cell membrane [77]. Moreover, it was found that the cytotoxicity determined by MTT assay was not disproportionately influenced by the complexes having different cellular uptake levels.

### Conclusion

The newly synthesized nickel(II) thiosemicarbazones were structurally characterized by various analytical, spectral,

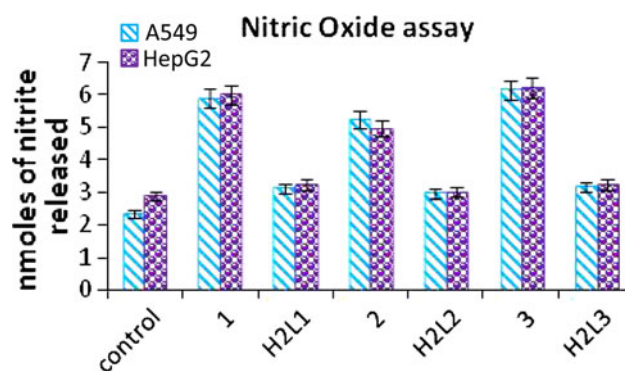


**Fig. 11** Nanomoles of nitrite released by the human cancer cell lines A549 and HepG2 after an incubation period of 48 h with the ligands (for A549, 17  $\mu\text{M}$   $\text{H}_2\text{L}^1$ , 20  $\mu\text{M}$   $\text{H}_2\text{L}^2$ , 15  $\mu\text{M}$   $\text{H}_2\text{L}^3$ ; for HepG2, 15  $\mu\text{M}$   $\text{H}_2\text{L}^1$ , 19  $\mu\text{M}$   $\text{H}_2\text{L}^2$ , 14  $\mu\text{M}$   $\text{H}_2\text{L}^3$ ) and complexes 1–3 (for A549, 10  $\mu\text{M}$  1, 8  $\mu\text{M}$  2, 10  $\mu\text{M}$  3; for HepG2, 8  $\mu\text{M}$  1, 7  $\mu\text{M}$  2, 8  $\mu\text{M}$  3). Error bars represent the standard error of the mean ( $n = 6$ )

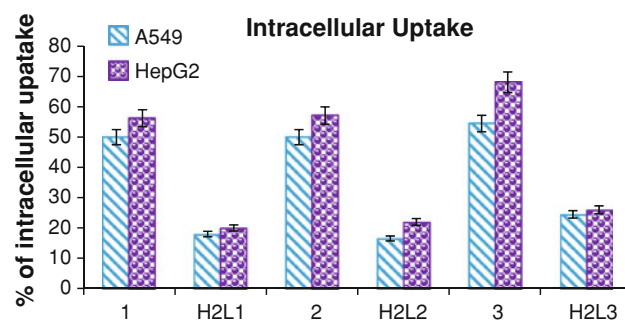
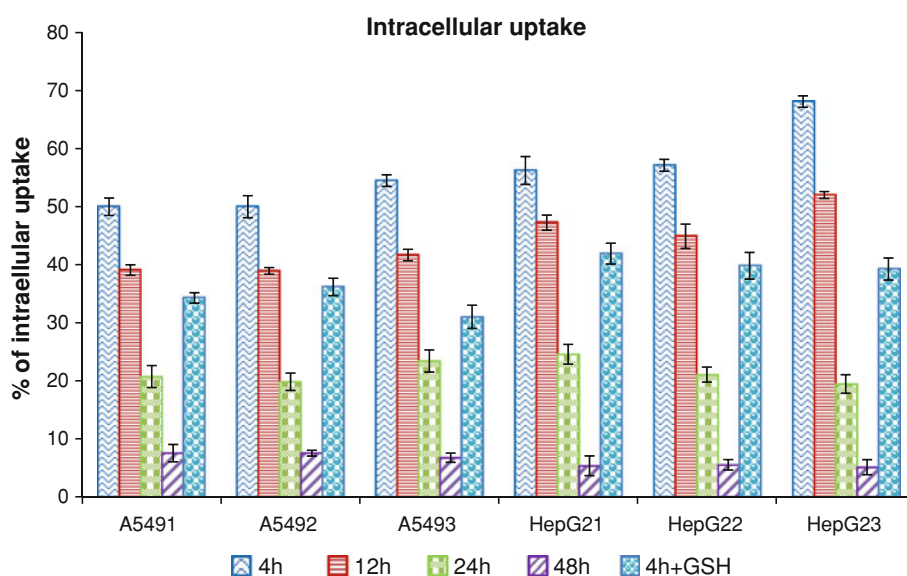


**Fig. 12** Percentage of intracellular uptake of the ligands (for A549, 17  $\mu\text{M}$   $\text{H}_2\text{L}^1$ , 20  $\mu\text{M}$   $\text{H}_2\text{L}^2$ , 15  $\mu\text{M}$   $\text{H}_2\text{L}^3$ ; for HepG2, 15  $\mu\text{M}$   $\text{H}_2\text{L}^1$ , 19  $\mu\text{M}$   $\text{H}_2\text{L}^2$ , 14  $\mu\text{M}$   $\text{H}_2\text{L}^3$ ) and complexes 1–3 (for A549, 10  $\mu\text{M}$  1, 8  $\mu\text{M}$  2, 10  $\mu\text{M}$  3; for HepG2, 8  $\mu\text{M}$  1, 7  $\mu\text{M}$  2, 8  $\mu\text{M}$  3) by human cancer cell lines A549 and HepG2 after an incubation period of 4 h. Error bars represent the standard error of the mean ( $n = 6$ )

and X-ray crystallographic techniques. From the X-ray analysis, it was found that in complexes 2 and 3, the ligand coordinated as a dibasic tridentate donor by forming a stable five-membered ring and a six-membered ring through phenolic oxygen, azomethine nitrogen, and thioate sulfur atoms. However, in complex 1, the ligand coordinated as a monobasic tridentate donor with phenolic oxygen, azomethine nitrogen, and thione sulfur atoms. The new complexes were subjected to studies of their potential biological properties such as cytotoxicity (MTT assay, LDH release, and nitric oxide assay) and cellular uptake along with free-radical scavenging and DNA binding studies. The complexes exhibited better binding with DNA, which was inferred from the greater magnitude of the binding constants. The cytotoxicity of the complexes in MTT assay showed that the complexes exhibited higher activity than their parent ligands and the conventional standard cisplatin in both cell lines used for the investigation. Correlating the activity of the complexes with their

**Fig. 13** Percentage of intracellular uptake of complexes **1–3** (for A549, 10  $\mu$ M **1**, 8  $\mu$ M **2**, 10  $\mu$ M **3**; for HepG2, 8  $\mu$ M **1**, 7  $\mu$ M **2**, 8  $\mu$ M **3**) by human cancer cell lines A549 and HepG2 after incubation periods of 4, 12, 24, and 48 h. Error bars represent the standard error of the mean ( $n = 6$ )



structures, we found that the increase in electron density on the metal increases the degree of cytotoxicity. In vivo cytotoxicity studies are under way to explore further the biological activities of the complexes.

### Supplementary material

Crystallographic data for **1**, **2**, and **3** have been deposited with the Cambridge Crystallographic Data Centre (CCDC) as supplementary publication nos. CCDC-678416, CCDC-678415, and CCDC-678417. The data can be obtained free of charge from <http://www.ccdc.cam.ac.uk/conts/retrieving.html> or from the CCDC (12 Union Road, Cambridge CB2 1EZ, UK; Fax: +44-1223-336033; e-mail: deposit@ccdc.cam.ac.uk).

**Acknowledgments** The authors gratefully acknowledge the Council of Scientific and Industrial Research (CSIR), New Delhi, India, and Department of Science and Technology (DST), India, for financial assistance. The reviewers are thanked for their valuable comments and suggestions enabling us to present this article in its current form.

### References

- Debra CQ, Kathy AK, Earl RK (2006) *Antiviral Res* 71:24–30
- Teitz Y, Ronen D, Vansover A, Stematsky T, Riggs JL (1994) *Antiviral Res* 24:305–314
- Arguelles MCR, Silva ECL, Sanmartin J, Pelagatti P, Zani F (2005) *J Inorg Biochem* 99:2231–2239
- Arguelles MCR, Silva ECL, Sanmartin J, Bacchi A, Pelizzi C, Zani F (2004) *Inorg Chim Acta* 357:2543–2552
- Cukurovali A, Yilmaz I, Gur S, Kazaz C (2006) *Eur J Med Chem* 41:201–207
- Murugkar A, Unnikrishnan B, Padhye S, Bhonde R, Teat S, Triantafyllou E, Sinn E (1999) *Met Based Drugs* 6:177–182
- Teitz Y, Barko N, Abramoff M, Ronen D (1994) *Chemotherapy (Tokyo)* 40:195–200
- Hu WX, Zhou W, Xia C, Wen X (2006) *Bioorg Med Chem Lett* 16:2213–2218
- Afrasiabi Z, Sinn E, Padhye S, Dutta S, Newton C, Anson CE, Powell AK (2003) *J Inorg Biochem* 95:306–314
- Bal T, Atasever B, Solakoglu Z, Kuruca SE, Ulkuseven B (2007) *Eur J Med Chem* 42:161–167
- Campana M, Laborie C, Barbier G, Assan R, Milcent R (1991) *Eur J Med Chem* 26:273–278
- Campbell MJ (1975) *Coord Chem Rev* 15:279–319
- Prabhakaran R, Huang R, Karvembu R, Jayabalakrishnan C, Natarajan K (2007) *Inorg Chim Acta* 360:691–694
- Prabhakaran R, Huang R, Renukadevi SV, Karvembu R, Zeller M, Natarajan K (2008) *Inorg Chim Acta* 361:2547–2552
- Prabhakaran R, Anantharaman S, Thilagavathi M, Kaveri MV, Kalaivani P, Karvembu R, Dharmaraj N, Bertagnolli H, Natarajan K (2011) *Spectrochim Acta* 78:844–853
- Prabhakaran R, Kalaivani P, Jayakumar R, Zeller M, Hunter AD, Renukadevi SV, Ramachandran E, Natarajan K (2011) *Metallomics* 3:42–48
- Prabhakaran R, Kalaivani P, Huang R, Sieger M, Kaim W, Viswanathamurthi P, Dallemer F, Natarajan K (2011) *Inorg Chim Acta* 376:317–324
- Kalaivani P, Prabhakaran R, Ramachandran E, Dallemer F, Paramaguru G, Renganathan R, Poornima P, Vijaya Padma V, Natarajan K (2012) *Dalton Trans* 41:2486–2499
- Prabhakaran R, Kalaivani P, Poornima P, Dallemer F, Paramaguru G, Vijaya Padma V, Renganathan R, Natarajan K (2012) *Dalton Trans* 41:9323–9336
- Chen J, Huang YW, Liu G, Afrasiabi Z, Sinn E, Padhye S, Ma Y (2004) *Toxicol Appl Pharmacol* 197:40–48
- Zheng LM, Li J, King I, Doyle TW, Chen SH (2001) *Curr Med Chem* 8:121–133
- Hall MD, Salam NK, Hellawell JL, Fales HM, Kensler CB, Ludwig JA, Szakacs G, Hibbs DE, Gottesman MM (2009) *J Med Chem* 52:3191–3204
- Gelasco A, Lippard SJ (1999) In: Clarke MJ, Sadler PJ (eds) *Topics in biological inorganic chemistry*, vol 1. Springer, New York, p 1
- Piper T, Borsky K, Keppler BK (1999) In: Clarke MJ, Sadler PJ (eds) *Topics in biological inorganic chemistry*, vol 1. Springer, New York, p 171

25. Reedijk J (2008) *Platinum Met Rev* 52:2–11
26. Hall MD, Okabe M, Shen DW, Liang XJ, Gottesman MM (2008) *Annu Rev Pharmacol Toxicol* 48:495–535
27. Gao X, Wang X, Ding J, Lin L, Li Y, Guo Z (2006) *Inorg Chem Commun* 9:722–726
28. Huq F, Yu JQ, Daghri H, Beale P (2004) *J Inorg Biochem* 98:1261–1270
29. Tayyem H, Huq F, Yu JQ, Beale P, Fisher K (2008) *Chem-MedChem* 3:145–151
30. Rabik CA, Dolan ME (2007) *Cancer Treat Rev* 33:9–23
31. Momekov G, Bakalova A, Karaivanova M (2005) *Curr Med Chem* 12:2177–2191
32. Zutphen SV, Reedijk J (2005) *Coord Chem Rev* 249:2845–2853
33. Purohit S, Kolay AP, Prasad LS, Manoharan PT, Ghosh S (1989) *Inorg Chem* 28:3735–3742
34. Venanzi J (1958) *J Chem Soc* 43:719–724
35. Vogel AI (1989) *Textbook of practical organic chemistry*, 5th edn. Longman, London
36. Sheldrick GM (1997) SHELXL-97, release 97–2. University of Göttingen, Göttingen
37. Wolfe A, Shimer GH, Meehan T (1987) *Biochemistry* 26:6392–6396
38. Cohen G, Eisenberg H (1969) *Biopolymers* 8:45–55
39. Blios MS (1958) *Nature* 26:1199–1200
40. Mossman T (1983) *J Immunol Methods* 65:55–63
41. Wacker WEC, Ulmer DD, Valee BL (1956) *J Med* 255:449–456
42. Stueher DJ, Marletta MA (1987) *J Immunol* 139:518–525
43. Xiong XB, Ma Z, Lai R, Lavasanifar A (2010) *Biomaterials* 31:757–768
44. West DX, Billeh IS, Jasinski JP, Jasinski JM, Butcher RJ (1998) *Transit Met Chem* 23:209–224
45. Prabhakaran R, Krishnan V, Pasumpon K, Sukanya D, Wendel E, Jayabalakrishnan C, Bertagnolli H, Natarajan K (2006) *Appl Organometal Chem* 20:203–213
46. Prabhakaran R, Renukadevi SV, Karvembu R, Huang R, Mautz J, Huttner G, Subashkumar R, Natarajan K (2008) *Eur J Med Chem* 43:268–273
47. Chikate RC, Padhye SB (2005) *Polyhedron* 24:1689–1700
48. Alomar K, Khan MA, Allain M, Bouet GM (2009) *Polyhedron* 28:1273–1280
49. Archaryya R, Basuli F, Peng SM, Lee GH, Falvello LR, Bhat-tacharya S (2006) *Inorg Chem* 45:1252–1259
50. Tojal JG, Dizarro JL, Orad AG, Sanz ARP, Ugaldia M, Diaz AA, Serra JL, Arriortua MI, Rojo T (2001) *J Inorg Biochem* 86:627–633
51. Naik AD, Annigeri SM, Gangadharmathy VB, Revankar VK, Mahale VB (2002) *J Mol Struct* 616:119–127
52. Rodrigues C, Batista AA, Aucélio RQ, Teixeira LR, Visentin LC, Beraldo H (2008) *Polyhedron* 27:3061–3066
53. Jouad EM, Riou A, Allain M, Khan MA, Bouet GM (2001) *Polyhedron* 20:67–74
54. Kalaivani P, Prabhakaran R, Dallemer F, Poornima P, Vaishnavi E, Ramachandran E, Vijaya Padma V, Renganathan R, Natarajan K (2012) *Metallomics* 4:101–113
55. Prabhakaran R, Sivasamy R, Angayarkanni J, Huang R, Kalaivani P, Karvembu R, Dallemer F, Natarajan K (2011) *Inorg Chim Acta* 374:647–653
56. Klayman DL, Scovill JP, Brtosevich JF, Bruce J (1983) *J Med Chem* 26:35–39
57. Prabhakaran R, Karvembu R, Hashimoto T, Shimizu K, Natarajan K (2005) *Inorg Chim Acta* 358:2093–2096
58. Ferrari MB, Capacchi S, Bisceglie F, Pelosi G, Tarasconi P (2001) *Inorg Chim Acta* 312:81–87
59. Fostiak LM, Gracia I, Swearinger JK, Bermejo E, Castineivas A, West DX (2003) *Polyhedron* 22:83–92
60. Hua LZ, Ying DC, Hui LJ, Jiang LY, Hua MY, Zeng YX (2000) *New J Chem* 24:1057–1062
61. Novakovi SB, Bogdanovic GA, Leovac VM (2005) *Inorg Chem Commun* 8:9–13
62. Hathaway BJ (1987) *Comprehensive coordination chemistry*, vol 5. Pergamon, Oxford
63. Patterson GS, Holm RH (1975) *Bioinorg Chem* 4:257–275
64. Kryatov SV, Mohanraj BS, Tarasov VV, Kryatova OP, Akimova EVR, Nuthakki B, Rusling JF, Staples RJ, Nazarenko AY (2002) *Inorg Chem* 41:923–930
65. Desbois MH, Astruc D (1989) *Organometallics* 8:1841–1847
66. Heinze J (1984) *Angew Chem Int Ed Engl* 23:831–847
67. Long EC, Barton JK (1990) *Acc Chem Res* 23:271–273
68. Pasternack RF, Gibbs EJ, Villafranca JJ (1983) *Biochemistry* 22:2406–2414
69. Selvi PT, Evans HS, Palanaindavar M (2005) *J Inorg Biochem* 99:2110–2118
70. Chauhan M, Arjmand F, Banerjee K (2007) *Inorg Chem* 46:3072–3082
71. Singh R, Singh S, Kumar S, Arora S (2007) *Food Chem* 103:1403–1410
72. Mahakunakoran P, Tohda M, Murakami Y, Matsumoto K, Watanabe H (2004) *Biol Pharm Bull* 27:38–46
73. Naik GH, Priyadarsini KI, Satav JG, Banavalikar MM, Sohoni PP, Biyani MK (2003) *Phytochemistry* 63:97–104
74. Rekka E, Kourounakis PN (1991) *J Pharm Pharmacol* 43:486–491
75. Pavanato A, Tunon MJ, Campos SS, Marroni CA, Llesuy S, Gallego JG, Marroni N (2003) *Dig Dis Sci* 48:824–829
76. Hartinger CG, Casini A, Duhot C, Tsybin YO, Messori L, Dyson PJ (2008) *J Inorg Biochem* 102:2136–2141
77. Prabhakaran R, Geetha A, Thilagavathi M, Karvembu R, Krishnan V, Bertagnolli H, Natarajan K (2004) *J Inorg Biochem* 98:2131–2140